Enriched virtual elements for plane elasticity with corner singularities

E. Artioli[*], L. Mascotto[†]

Abstract

We construct a nonconforming virtual element method for the approximation of singular solutions to isotropic linear elasticity problems on polygonal domains. Standard nonconforming virtual element spaces are enriched with suitable singular functions. The enrichment is based on the nonconforming structure of the discrete spaces and not on partition of unity techniques. We prove optimal convergence and assess numerically the theoretical results of the method. The proposed scheme naturally paves the way for an efficient linear elastic fracture solver.

AMS subject classification: 65N12; 65N15; 65N30

Keywords: Virtual element method; Extended Galerkin method; Singular function; Polygonal mesh; Linear elasticity

1 Introduction

Solutions to partial differential equations (PDEs) on polygonal and polyhedral domains are generally singular at vertices and edges. If the coefficients of a given elliptic PDE are constants, then it is possible to show an explicit splitting of the exact solution into a smooth contribution, and series of singular functions at the kinks of the domain. Classical monographs discussing the singular behaviour of the solution are [16, 20, 24], while general techniques to derive explicit asymptotic expansions are given in [22, 23, 27]. Other works related to singular expansion for the isotropic linear elasticity case are due to Costabel and Dauge [13–15] and Rössle [30]. The last reference contains singular expansion for all possible types of boundary conditions.

A possible way to approximate solutions to PDEs is to use Galerkin methods. The rate of convergence of a Galerkin method is dictated by the minimum between the polynomial degree of accuracy of the method, e.g., the polynomial degree in finite elements, and a parameter related to the Sobolev regularity of the exact solution. Therefore, the rate of convergence of a Galerkin method is typically suboptimal, as solutions to PDEs are singular in some parts of the domain.

For this reason, several Galerkin methods based on polynomial spaces enriched with singular functions have been developed over the years. To the best of our knowledge, the inclusion of singular functions in a Galerkin framework traces back to the pioneering works by Fix and collaborators [17, 18] at the end of the 60ies for quadrilateral meshes; the extension to triangular meshes is due to Whiteman and collaborators [5] in the 70ies. Enriched elements fell into forgetfulness for several years and were re-discovered by Belytschko and collaborators [28] (the extended finite element method, XFEM) and Babuška and collaborators [31] (the generalized finite element method, GFEM). Roughly speaking the above approaches are based on the same idea: special singular functions are added to the usual polynomial approximation space testing them with "hat functions", i.e., singular functions are localized by multiplying them with some cut-off polynomial functions already contained in the original space. The extension of the works by Belytschko et al. to the case of polytopal meshes is given in [8, 9]. The above approaches lead to approximation

[*]Dipartimento di Ingegneria "Enzo Ferrari", Università degli Studi di Modena e Reggio Emilia, 41121 Modena, Italy (edoardo.artioli@unimore.it)

[†]Dipartimento di Matematica e Applicazioni, Università degli Studi di Milano-Bicocca, Via R. Cozzi, 55 - 20125 Milano, Italy (lorenzo.mascotto@unimib.it); IMATI-CNR, Pavia, Italy; Fakultät für Mathematik, Universität Wien, 1090 Vienna, Austria

spaces that are globally continuous with basis functions shared by possibly many elements, leading to a loss of the sparsity of the matrix stemming from the method.

Another possible enrichment is based on employing discrete spaces of discontinuous polynomials enhanced by singular functions; see, e.g., the celatus discontinuous Galerkin method in [19]. The advantage of this approach is that the enrichment of the space is quite easy and the support of the singular functions is only one element, at the price of losing the global continuity of the discrete solution.

A third and more recent approach lies in between the two discussed above. It hinges upon using enriched nonconforming virtual element spaces (ncVEM) and was designed for the approximation of singular solutions to the Poisson problem in [3]; the ideas in this reference were later extended to the hybrid high-order method in [32]. Standard nonconforming virtual element spaces consist of solutions to local elliptic problems with polynomial data. Their enriched version has the same structure with the difference that boundary conditions are polynomials plus suitable singular functions. This construction allows for an automatic inclusion of the singular functions in the space.

Compared to the standard XFEM and GFEM, the support of local functions in enriched ncVEM is smaller and is contained in at most two elements. Compared to "celatus methods", discrete functions are not fully discontinuous. Moreover, as discussed in [3, Appendix B], the structure of the discrete spaces naturally offers a framework that allows for orthogonalization procedures that improve the ill-conditioning of the final system; such techniques are not immediately replicable in the other two settings. These advantages come at the price that virtual element functions are not know in closed form but only through certain degrees of freedom. In other words, an explicit representation of the virtual element functions is only possible through projectors onto certain enriched polynomial spaces.

The goal of this paper is to construct an enriched nonconforming virtual element method for isotropic linear elasticity problems on polygons. We shall design the method, analyse optimal convergence error estimates, and assess the theoretical findings with some test cases.

Structure of the paper. We introduce the model problem and discuss the singular behaviour at vertices in Section 2. We construct the enriched ncVEM in Section 3 and discuss the convergence analysis in Section 4. Numerical results are presented in Section 5 and conclusions are drawn in Section 6. In Appendix A, we review in details the singular behaviour of solutions to isotropic linear elasticity problems on polygons.

Notation. Given a domain D in $\mathbb{R}^2$, $H^s(D)$ denotes the Sobolev space of order s in $\mathbb{N}$ over D. The case $s = 0$ coincides with the Lebesgue space $L^2(D)$. Sobolev spaces of positive noninteger order s are constructed using interpolation theory. We endow $H^s(D)$ with the usual seminorm, norm, and inner products

$$|\cdot|_{s,D}, \qquad \|\cdot\|_{0,D}, \qquad (\cdot,\cdot)_{0,D}.$$

Given ∂D the boundary of D, $H^{\frac{1}{2}}(\partial D)$ denotes the space of traces of $H^1(D)$ functions over ∂D, which we can endow with the usual Aronszajin-Gagliardo-Slobodeckij norm. The spaces $H^{-s}(D)$, $s > 0$, and $H^{-\frac{1}{2}}(\partial D)$ are defined by duality.

Throughout, we shall employ standard notation for differential operators. For instance, ∇, div, and $\mathscr{E}$ denote the usual gradient, divergence, and symmetric gradient operators.

2 Model problem and regularity of the solution

Given the (constant) Lamé parameters μ and λ, introduce the elasticity operator

$$\mathbf{M}\cdot := \mu \mathrm{div}\mathscr{E}\cdot + (\mu+\lambda)\nabla \mathrm{div}\cdot. \tag{1}$$

Let Ω in $\mathbb{R}^2$ be a polygonal domain with boundary Γ and $\mathbf{f}$ be in $[L^2(\Omega)]^2$. The domain Ω can contain slits. We consider the isotropic linear elasticity problem

$$\begin{cases} -\mathbf{M}\mathbf{u} = \mathbf{f} & \text{in } \Omega \\ \mathbf{u} = \mathbf{0} & \text{on } \partial\Omega. \end{cases} \tag{2}$$

Introduce

$$\mathbf{V} := [H_0^1(\Omega)]^2, \quad a(\mathbf{u},\mathbf{v}) := \mu \int_\Omega \mathscr{E}(\mathbf{u}) : \mathscr{E}(\mathbf{v}) + (\mu+\lambda) \int_\Omega \mathrm{div}\mathbf{u}\, \mathrm{div}\mathbf{v},$$

and the energy norm

$$|\mathbf{v}|^2 := a(\mathbf{v},\mathbf{v}) \qquad \forall \mathbf{v} \in \mathbf{V}.$$

A weak formulation of problem (2) reads

$$\begin{cases} \text{find } \mathbf{u} \in \mathbf{V} \text{ such that} \\ a(\mathbf{u},\mathbf{v}) = (\mathbf{f},\mathbf{v})_{0,\Omega} \qquad \forall \mathbf{v} \in \mathbf{V}. \end{cases} \tag{3}$$

Problem (3) is well posed due to the Lax-Milgram lemma, which holds true based on Korn's inequality; see, e.g., [11, Chapter 11]. In general, the solution $\mathbf{u}$ to (3) belongs to $\mathbf{V}$ but has finite Sobolev regularity at the vertices of Ω.

It is known [16, 20] that the solution $\mathbf{u}$ to (3) is given by the sum of a smooth term $\mathbf{u}_0$ and a term $\mathscr{S}$ that is singular at the vertices of Ω:

$$\mathbf{u} = \mathbf{u}_0 + \mathscr{S}. \tag{4}$$

In the simplest case, given (r,θ) the polar coordinates centred at a vertex $\mathbf{A}$, $\mathscr{S}$ around a neighbourhood of $\mathbf{A}$ is a series of functions of the form

$$r^\alpha(\mathscr{S}_1(\theta), \mathscr{S}_2(\theta))^T, \tag{5}$$

for positive factors α that depend on the angle at $\mathbf{A}$, and the Lamé parameters.

In Appendix A below, we review examples of singular solutions $\mathscr{S}$, and discuss the singular exponent α and the smooth angular part $(\mathscr{S}_1(\theta), \mathscr{S}_2(\theta))$. The crucial property satisfied by $\mathscr{S}$ is that the singular functions belong to the kernel of the isotropic elasticity operator $\mathbf{M}$, i.e., they represent singular displacement field corresponding to self-equilibrated stress states for the material body

$$\mathbf{M}\mathscr{S} = \mathbf{0}. \tag{6}$$

3 The enriched virtual element method for isotropic linear elasticity

We design a nonconforming enriched virtual element method for the approximation of solutions to the isotropic linear elasticity problem (3). For the sake of presentation, we henceforth assume that $\mathscr{S}$ in (4) consists of only one term $\mathscr{S}_\mathbf{A}$ that is singular at a vertex $\mathbf{A}$ of Ω and has the form (5). In particular, for a given smooth field $\mathbf{u}_0$, we write

$$\mathbf{u} = \mathbf{u}_0 + \mathscr{S}_\mathbf{A}. \tag{7}$$

The remainder of this section is organized as follows: in Section 3.1, we introduce admissible sequences of meshes and enriched polynomial spaces; in Section 3.2, we construct nonconforming enriched virtual element spaces for isotropic linear elasticity; in Section 3.3, we study the interpolation properties of functions in such virtual element spaces; in Section 3.4, we design and analyse the properties of the discrete bilinear form and right-hand side; in Section 3.5, we present the virtual element method and discuss its well posedness.

3.1 Meshes: layerizations and enriched polynomial spaces

We consider a mesh $\mathscr{T}_n$ that possibly contains elements with slits. By $\mathscr{E}_n$, we denote the corresponding set of edges, which we split into internal $\mathscr{E}_n^I$ and boundary $\mathscr{E}_n^B$ edges. Given $K \in \mathscr{T}_n$, its set of edges is $\mathscr{E}^K$; its outward pointing normal vector is $\mathbf{n}_K$; its centroid is $\mathbf{x}^K$; its diameter is h_K; its number of vertices is N_V^K. Given $e \in \mathscr{E}_n$, its centroid is $\mathbf{x}^e$ and its length is h_e; further, we associate to e a normal unit vector $\mathbf{n}_e$ once and for all. Clearly, if $e \in \mathscr{E}^K$ for some $K \in \mathscr{T}_n$, then we have $\mathbf{n}_K \cdot \mathbf{n}_e = \pm 1$.

We assume that there exists a uniform $\gamma \in (0,1)$ such that

(**A0**) for all K_1 and K_2 in $\mathscr{T}_n$ with $\overline{K_1} \cup \overline{K_2} \neq \emptyset$, $\gamma h_{K_1} \leq h_{K_2} \leq \gamma^{-1} h_{K_1}$;

(**A1**) every K in $\mathscr{T}_n$ is star-shaped with respect to a ball of radius larger than or equal to γh_K;

(**A2**) no small edges are allowed, i.e, for all $K \in \mathscr{T}_n$ and $e \in \mathscr{E}^K$, $\gamma h_K \leq h_e$.

We introduce element and edge layers. First, we recall decomposition (7) and that the singular function $\mathscr{S}_{\mathbf{A}}$ is singular only at the vertex $\mathbf{A}$. Given the polygonal mesh $\mathscr{T}_n$, we introduce the first layer of elements either abutting or close to vertex $\mathbf{A}$: given a positive parameter $\widetilde{\gamma}$,

$$\mathscr{T}_n^1 := \{K \in \mathscr{T}_n \mid \operatorname{dist}(\mathbf{A}, K) \leq \widetilde{\gamma} \operatorname{diam}(\Omega)\}. \tag{8}$$

Next, we define the second layer, i.e., the set of elements abutting the elements in $\mathscr{T}_n^1$:

$$\mathscr{T}_n^2 := \left\{K \in \mathscr{T}_n \mid \exists \widetilde{K} \in \mathscr{T}_n^1 \text{ such that } \overline{K} \cap \overline{\widetilde{K}} \subset \mathscr{E}_n\right\}.$$

Eventually, we introduce the layer of the remaining elements:

$$\mathscr{T}_n^3 := \mathscr{T}_n \setminus (\mathscr{T}_n^1 \cup \mathscr{T}_n^2).$$

We also consider a layerization of the edges $\mathscr{E}_n$. Notably, we define

$$\mathscr{E}_n^1 := \left\{e \in \mathscr{E}_n \mid \exists K \in \mathscr{T}_n^1 \text{ such that } e \in \mathscr{E}^K\right\}, \qquad \mathscr{E}_n^2 := \mathscr{E}_n \setminus \mathscr{E}_n^1.$$

We give a graphical example of the element and edge layers on the slit domain

$$\Omega := (0,1)^2 \setminus \{(x,y) \in \mathbb{R}^2 \mid x = y,\ x \in (1/4, 3/4)\}.$$

The singular vertex $\mathbf{A}$ is the tip $(3/4, 3/4)$ and $\widetilde{\gamma}$ is set to 0.1.

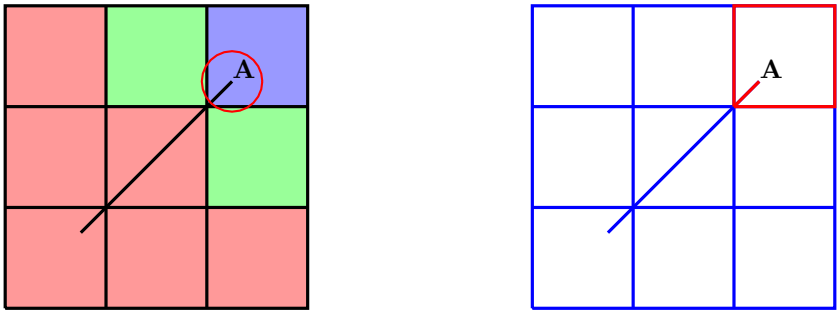

Figure 1: *Left panel*: in blue, the elements in the first element layer $\mathscr{T}_n^1$; in green, the elements in the second element layer $\mathscr{T}_n^2$; in red, the elements in the third layer $\mathscr{T}_n^3$. *Right panel*: in red, the edges in the first edge layer $\mathscr{E}_n^1$; in blue, the edges in the second edge layer $\mathscr{E}_n^2$. The domain is a unit square domain with an internal crack. We assume that the solution to problem (3) is singular only at the right-upper tip of the crack $\mathbf{A} = (3/4, 3/4)$. In red, we depict the circumference of radius 0.1 centred at $\mathbf{A}$. The parameter $\widetilde{\gamma}$ in (8) is 0.1.

Next, given the singular function $\mathscr{S}_{\mathbf{A}}$ in polar coordinates (r, θ) centred at $\mathbf{A}$, we define

$$\mathscr{S}_{\mathbf{A}}^K(r,\theta) := \mathscr{S}_{\mathbf{A}}\left(\frac{r}{h_K}, \theta\right), \qquad \mathscr{S}_{\mathbf{A}}^e(r,\theta) := \mathscr{S}_{\mathbf{A}}\left(\frac{r}{h_e}, \theta\right).$$

Given $K \in \mathscr{T}_n$ and $e \in \mathscr{E}^K$, introduce the element and edge "elasticity" trace operators $\gamma^e_{\rm El}$, $\gamma^K_{\rm El}$: $[H^1(K)]^2 \to [H^{-\frac{1}{2}}(\partial K)]^2$ on $K \in \mathscr{T}_n$ as

$$\gamma^K_{\rm El}(\mathbf{v}) := \mu(\mathscr{E}\mathbf{v})\mathbf{n}_K + (\mu+\lambda){\rm div}\mathbf{v}\ \mathbf{n}_K \quad \gamma^e_{\rm El}(\mathbf{v}) := \mu(\mathscr{E}\mathbf{v})\mathbf{n}_e + (\mu+\lambda){\rm div}\mathbf{v}\ \mathbf{n}_e \quad \forall \mathbf{v} \in [H^1(K)]^2. \tag{9}$$

We define (possibly) enriched polynomial spaces over elements and edges as follows. For a given p in $\mathbb{N}$, we set $\mathbf{P}_p(K)$ and $\mathbf{P}_p(e)$ as the spaces of polynomial fields over K and e. We define

$$\widetilde{\mathbf{P}}_p(K) := \begin{cases} \mathbf{P}_p(K) \oplus \mathscr{S}^K_{\mathbf{A}} & \text{if } K \in \mathscr{T}^1_n \\ \mathbf{P}_p(K) & \text{if } K \in \mathscr{T}^2_n \cup \mathscr{T}^3_n. \end{cases} \qquad \widetilde{\mathbf{P}}_p(e) := \begin{cases} \mathbf{P}_p(e) \oplus \gamma^e_{\rm El}(\mathscr{S}^e_{\mathbf{A}}) & \text{if } e \in \mathscr{E}^1_n \\ \mathbf{P}_p(e) & \text{if } e \in \mathscr{E}^2_n. \end{cases}$$

3.2 Nonconforming enriched virtual elements

Recall that the elasticity operator $\mathbf{M}$ and the trace elasticity operator $\gamma^K_{\rm El}$ are defined in (1) and (9), respectively. We define the local enriched virtual element space on the element K as follows:

$$\mathbf{V}_n(K) := \left\{ \mathbf{v}_n \in [H^1(K)]^2 \mid \mathbf{M}(\mathbf{v}_n) \in \mathbf{P}_{p-2}(K),\ \gamma^K_{\rm El}(\mathbf{v}_n)_{|e} \in \widetilde{\mathbf{P}}_{p-1}(e)\, \forall e \in \mathscr{E}^K \right\}. \tag{10}$$

Thanks to (6), we have the inclusion

$$\widetilde{\mathbf{P}}_p(K) \subset \mathbf{V}_n(K).$$

The above inclusion guarantees optimal approximation properties of the space; see Lemma 4.3 below.

Consider the following set of linear functionals:

- the bulk moment: given any basis $\{\mathbf{m}^K_\alpha\}_{\alpha=1}^{\dim(\mathbf{P}_{p-2}(K))}$ of $\mathbf{P}_{p-2}(K)$,

$$|K|^{-1} \int_K \mathbf{v}_n \cdot \mathbf{m}^K_\alpha \qquad \forall \alpha = 1, \dots, \dim(\mathbf{P}_{p-2}(K)); \tag{11}$$

- the polynomial edge moments: for each $e \in \mathscr{E}^K$, given a basis $\{\mathbf{m}^e_\alpha\}_{\alpha=1}^{\dim(\mathbf{P}_{p-1}(e))}$ of $\mathbf{P}_{p-1}(e)$,

$$|e|^{-1} \int_e \mathbf{v}_n \cdot \mathbf{m}^e_\alpha \qquad \forall e \in \mathscr{E}^K,\ \forall \alpha = 1, \dots, \dim(\mathbf{P}_{p-1}(e)); \tag{12}$$

- the "singular" edge moments: for each "singular" edge $e \in \mathscr{E}^1_n$,

$$\int_e \mathbf{v}_n \cdot \gamma^K_{\rm El}(\mathscr{S}_{\mathbf{A}})_{|e} \qquad \forall e \in \mathscr{E}^K. \tag{13}$$

Define the local bilinear form

$$a^K(\mathbf{u}, \mathbf{v}) := \mu(\nabla\mathbf{u}, \nabla\mathbf{v})_{0,K} + (\mu+\lambda)({\rm div}\mathbf{u}, {\rm div}\mathbf{v})_{0,K} \qquad \forall K \in \mathscr{T}_n.$$

Lemma 3.1. *The set of degrees of freedom* (11)–(12)–(13) *is unisolvent.*

Proof. The proof follows along the same lines as those of [3, Lemma 3.1]. The dimension of $\mathbf{V}_n(K)$ matches the number of degrees of freedom, whence we only need to check their unisolvence.

Given $\mathbf{v}_n \in \mathbf{V}_n(K)$ such that all the functionals (11)–(12)–(13) vanish, we show that

$$a^K(\mathbf{v}_n, \mathbf{v}_n) = 0. \tag{14}$$

In fact, if this is the case, then we use the Korn's inequality [11, Corollary 11.2.22] and deduce that $\mathbf{v}_n$ is a constant vector. The assertion follows imposing zero vector average, e.g., on an edge.

To show (14), we use an integration by parts and the definition of $\mathbf{V}_n(K)$ in (10)

$$a^K(\mathbf{v}_n, \mathbf{v}_n) = -(\mathbf{v}_n, \underbrace{\mathbf{M}\mathbf{v}}_{\in \mathbf{P}_{p-2}(K)})_{0,K} + \sum_{e \in \mathscr{E}^K} (\mathbf{v}_n, \underbrace{\gamma^K_{\rm El}(\mathbf{v}_n)}_{\widetilde{\mathbf{P}}_{p-1}(e)})_{0,e} \overset{(10)}{=} 0.$$

□

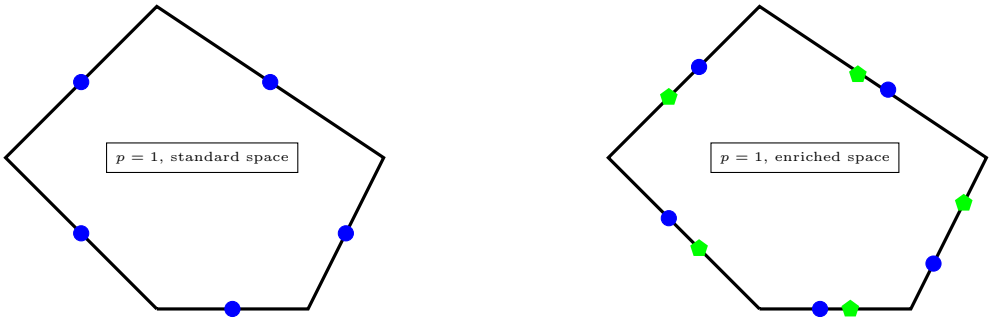

Figure 2: Degrees of freedom on a pentagon for $p = 1$. *Left panel*: standard nonconforming VEM. *Right panel*: enriched nonconforming VEM. The blue circles represent the standard edge polynomial moments (12). The green pentagons represent the enriched edge moments (13).

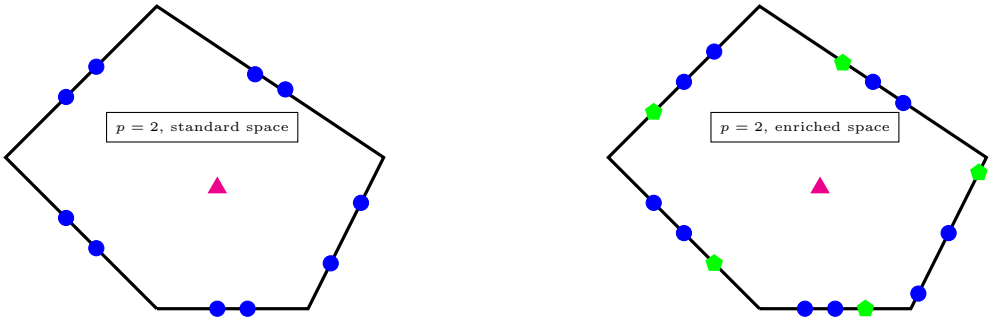

Figure 3: Degrees of freedom on a pentagon for $p = 2$. *Left panel*: standard nonconforming VEM. *Right panel*: enriched nonconforming VEM. The blue circles represent the standard edge polynomial moments (12). The green pentagons represent the enriched edge moments (13). The magenta triangle represents the bulk polynomial moments (11).

In Figures 2 and 3, we depict the degrees of freedom for standard and enriched nonconforming virtual elements on a pentagon for $p = 1$ and 2, respectively.

The set of standard degrees of freedom (11)–(12) could be used to construct a standard polynomial nonconforming virtual element space for the isotropic linear elasticity problem. The resulting construction would differ from those available in the literature; see, e.g., [33].

Next, we construct the global nonconforming space. To the aim, define the vector broken Sobolev space with respect to the decomposition $\mathscr{T}_n$ as follows:

$$[H^1(\mathscr{T}_n)]^2 := \left\{ \mathbf{v} \in [L^2(\Omega)]^2 \mid \mathbf{v}_{|K} \in [H^1(K)]^2 \; \forall K \in \mathscr{T}_n \right\}.$$

For each edge e in $\mathscr{E}_n$, recall that $\mathbf{n}_e$ is a fixed-once-and-for all normal unit vector of e. Given an internal edge e in $\mathscr{E}_n^I$, denote the two adjacent elements by K_1 and K_2. If instead e in $\mathscr{E}_n^B$ is a boundary edge, let K be the only element such that e in $\mathscr{E}^K$.

We define the jump operator as follows:

$$[\![\mathbf{v}]\!]_e = [\![\mathbf{v}]\!] := \begin{cases} \mathbf{v}_{|K_1} \cdot \mathbf{n}_{K_1} + \mathbf{v}_{|K_2} \cdot \mathbf{n}_{K_2} & \text{if } e \in \mathscr{E}_n^I \\ \mathbf{v}_{|K} \cdot \mathbf{n}_K & \text{if } e \in \mathscr{E}_n^B \end{cases} \qquad \forall \mathbf{v} \in [H^1(\mathscr{T}_n)]^2.$$

We define a (vector) nonconforming Sobolev space with respect to $\mathscr{T}_n$:

$$[H_p^{1,nc}(\mathscr{T}_n)]^2 := \left\{ \mathbf{v} \in [H^1(\mathscr{T}_n)]^2 \middle| \int_e ([\![\mathbf{v}]\!] \; \mathbf{n}_e) \cdot \widetilde{\mathbf{m}}^e = 0 \; \forall e \in \mathscr{E}_n, \; \forall \widetilde{\mathbf{m}}^e \in \widetilde{\mathbf{P}}_{p-1}(e) \right\}. \tag{15}$$

Eventually, we define the global nonconforming vector enriched virtual element space for isotropic linear elasticity as follows:

$$\mathbf{V}_n := \left\{ \mathbf{v}_n \in [H_p^{1,nc}(\mathscr{T}_n)]^2 \mid \mathbf{v}_{n|K} \in \mathbf{V}_n(K) \; \forall K \in \mathscr{T}_n \right\}.$$

We endow the space $\mathbf{V}_n$ with a set of degrees of freedom obtained by a standard nonconforming coupling of the edge moments (12) and (13).

3.3 Interpolation estimates

We analyse interpolation estimates by means of functions in the global virtual element space $\mathbf{V}_n$. Introduce the broken energy bilinear form

$$a^{\mathscr{T}_n}(\mathbf{u},\mathbf{v}) := \sum_{K\in\mathscr{T}_n} a^K(\mathbf{u},\mathbf{v}) \qquad\qquad \forall \mathbf{u},\ \mathbf{v}\in[H^1(\mathscr{T}_n)]^2,$$

and the broken, global and local energy norm

$$|\mathbf{v}|^2_{a^{\mathscr{T}_n}} := a^{\mathscr{T}_n}(\mathbf{v},\mathbf{v}) = \sum_{K\in\mathscr{T}_n} |\mathbf{v}|^2_{a^K} := \sum_{K\in\mathscr{T}_n} a^K(\mathbf{v},\mathbf{v}) \qquad\qquad \forall \mathbf{v}\in[H^1(\mathscr{T}_n)]^2.$$

Proposition 3.2. *Let $\mathbf{u}\in[H^{s+1}(\Omega)]^2$, $s>0$. Then, there exists $\mathbf{u}_I\in\mathbf{V}_n$ such that, for all $\mathbf{u}_\pi$ piecewise in $[\widetilde{\mathbf{P}}_p(K)]^2$,*

$$|\mathbf{u}-\mathbf{u}_I|_{a^{\mathscr{T}_n}} \le |\mathbf{u}-\mathbf{u}_\pi|_{a^{\mathscr{T}_n}}.$$

Proof. The proof follows along the same lines as that of [26, Proposition 3.8] and [3, Lemma 4.3].

Define $\mathbf{u}_I$ such that, for all the degrees of freedom dof of $\mathbf{V}_n$,

$$\mathrm{dof}(\mathbf{u}-\mathbf{u}_I)=0. \tag{16}$$

Using an integration by parts, definition (16) with the properties of (10), an integration by parts back, and the Cauchy-Schwarz inequality yield, for all K in $\mathscr{T}_n$,

$$\begin{aligned}
|\mathbf{u}-\mathbf{u}_I|^2_{a^K} &= -(\mathbf{u}-\mathbf{u}_I,\mathbf{M}(\mathbf{u}-\mathbf{u}_I))_{0,K} + \sum_{e\in\mathscr{E}^K}(\mathbf{u}-\mathbf{u}_I,\gamma^K_{\mathrm{El}}(\mathbf{u}-\mathbf{u}_I))_{0,e}\\
&= -(\mathbf{u}-\mathbf{u}_I,\mathbf{M}(\mathbf{u}-\mathbf{u}_\pi))_{0,K} + \sum_{e\in\mathscr{E}^K}(\mathbf{u}-\mathbf{u}_I,\gamma^K_{\mathrm{El}}(\mathbf{u}-\mathbf{u}_\pi))_{0,e}\\
&= a^K(\mathbf{u}-\mathbf{u}_I,\mathbf{u}-\mathbf{u}_\pi) \le |\mathbf{u}-\mathbf{u}_I|_{a^K}|\mathbf{u}-\mathbf{u}_\pi|_{a^K}.
\end{aligned}$$

Diving both sides by $|\mathbf{u}-\mathbf{u}_I|_{a^K}$ and summing over all the elements yield the assertion. □

3.4 Discrete bilinear forms and right-hand side

We construct the discrete computable bilinear forms and right-hand side.

The discrete bilinear form. Let $\mathbb{RM}(K)$ be the space of the rigid body motions over K. We define an energy projector into enriched polynomials $\widetilde{\mathbf{\Pi}}^{a,K}_p = \widetilde{\mathbf{\Pi}}^a_p : [H^1(K)]^2 \to \widetilde{\mathbf{P}}_p(K)$ as follows:

$$\begin{cases} a^K(\widetilde{\mathbf{q}}_p, \mathbf{v}-\widetilde{\mathbf{\Pi}}^a_p\mathbf{v}) = 0\\ \int_{\partial K}(\mathbf{v}-\widetilde{\mathbf{\Pi}}^a_p\mathbf{v})q_{\mathbb{RM}} = \mathbf{0} \end{cases} \qquad \forall\widetilde{\mathbf{q}}_p\in\widetilde{\mathbf{P}}_p(K),\quad \forall\mathbf{v}\in[H^1(K)]^2,\quad \forall q_{\mathbb{RM}}\in\mathbb{RM}(K). \tag{17}$$

Lemma 3.3. *Given $\mathbf{v}_n\in\mathbf{V}_n$, $\widetilde{\mathbf{\Pi}}^a_p\mathbf{v}_n$ is computable explicitly via the degrees of freedom* (11), (12), *and* (13).

Proof. As for the "bulk" contribution, we have to show the computability of $a^K(\widetilde{\mathbf{q}}_p,\mathbf{v}_n)$ for all $\widetilde{\mathbf{q}}_p\in\mathbf{P}_p(K)$ and $\mathbf{v}_n\in\mathbf{V}_n$:

$$a^K(\widetilde{\mathbf{q}}_p,\mathbf{v}_n) = -(\underbrace{\mathbf{M}\widetilde{\mathbf{q}}_p}_{\in\mathbf{P}_{p-2}(K)},\mathbf{v}_n)_{0,K} + \sum_{e\in\mathscr{E}^K}(\underbrace{\gamma^K_{\mathrm{El}}(\widetilde{\mathbf{q}}_p)}_{\in\widetilde{\mathbf{P}}_{p-1}(e)},\mathbf{v}_n)_{0,e}.$$

The fact that $\mathbf{M}\widetilde{\mathbf{q}}_p\in\mathbf{P}_{p-2}(K)$ follows from (6). The first and second terms on the right-hand side are computable via the degrees of freedom (11), and (12)-(13), respectively. The computability of the boundary constraint in (17) follows from the definition of the edge moments (12)–(13). □

Following the VEM gospel [6], we use the energy projection $\widetilde{\mathbf{\Pi}}_p^a$ to design the discrete bilinear form, mimicking the continuous one $a(\cdot,\cdot)$:

$$a_n(\mathbf{u}_n,\mathbf{v}_n) := \sum_{K\in\mathscr{T}_n} a_n^K(\mathbf{u}_n,\mathbf{v}_n) \qquad\qquad \forall \mathbf{u}_n,\, \mathbf{v}_n \in \mathbf{V}_n,$$

where

$$a_n^K(\mathbf{u}_n,\mathbf{v}_n) := a^K(\widetilde{\mathbf{\Pi}}_p^a\mathbf{u}_n,\widetilde{\mathbf{\Pi}}_p^a\mathbf{v}_n) + S^K((\mathbf{I}-\widetilde{\mathbf{\Pi}}_p^a)\mathbf{u}_n,(\mathbf{I}-\widetilde{\mathbf{\Pi}}_p^a)\mathbf{v}_n) \qquad \mathbf{u}_n,\, \mathbf{v}_n \in \mathbf{V}_n(K). \tag{18}$$

The bilinear form $S^K : \ker(\widetilde{\mathbf{\Pi}}_p^a)\times\ker(\widetilde{\mathbf{\Pi}}_p^a)\to\mathbb{R}$ in (18) must be computable from the degrees of freedom and is such that there exist two positive constants $c_*\le c^*$ independent of the discretisation parameters with

$$c_* a^K(\mathbf{v}_n,\mathbf{v}_n) \le S^K(\mathbf{v}_n,\mathbf{v}_n) \le c^* a^K(\mathbf{v}_n,\mathbf{v}_n) \qquad\qquad \forall \mathbf{v}_n\in\ker(\widetilde{\mathbf{\Pi}}_p^a). \tag{19}$$

Given $\alpha_* := \min(1,c_*)$ and $\alpha^* := \max(1,c^*)$, it can be shown that

$$\alpha_* a^K(\mathbf{v}_n,\mathbf{v}_n) \le a_n^K(\mathbf{v}_n,\mathbf{v}_n) \le \alpha^* a^K(\mathbf{v}_n,\mathbf{v}_n) \qquad\qquad \forall \mathbf{v}_n\in\ker(\widetilde{\mathbf{\Pi}}_p^a),\ \forall K\in\mathscr{T}_n. \tag{20}$$

On each element K in $\mathscr{T}_n$, we have the consistency property

$$a_n^K(\widetilde{\mathbf{q}}_p,\mathbf{v}_n) = a^K(\widetilde{\mathbf{q}}_p,\mathbf{v}_n) \qquad\qquad \forall \widetilde{\mathbf{q}}_p\in\widetilde{\mathbf{P}}_p(K), \quad \forall \mathbf{v}_n\in\mathbf{V}_n(K). \tag{21}$$

Next, we exhibit an explicit choice for the stabilization and prove the related bounds in (19).

An explicit choice for the stabilization. Given e in $\mathscr{E}^K$ an edge of an element K in $\mathscr{T}_n$, introduce the enriched L^2-edge polynomial projection $\widetilde{\mathbf{\Pi}}_{p-1}^{0,e} : [L^2(e)]^2 \to \widetilde{\mathbf{P}}_{p-1}(e)$ defined as

$$(\widetilde{\mathbf{q}}_{p-1}^e, \widetilde{\mathbf{\Pi}}_{p-1}^{0,e}\mathbf{v}-\mathbf{v})_{0,e} \qquad\qquad \forall \widetilde{\mathbf{q}}_{p-1}^e\in\widetilde{\mathbf{P}}_{p-1}(e),\ \forall \mathbf{v}\in[L^2(e)]^2. \tag{22}$$

This operator is computable for functions in $\mathbf{V}_n$ from their standard and "singular" edge degrees of freedom (12)–(13).

Furthermore, given K in $\mathscr{T}_n$, introduce the standard L^2-bulk polynomial projection $\mathbf{\Pi}_{p-2}^0 : [L^2(K)]^2 \to \mathbf{P}_{p-2}(K)$ defined as

$$(\mathbf{q}_{p-2}, \mathbf{\Pi}_{p-2}^0\mathbf{v}-\mathbf{v})_{0,K} \qquad\qquad \forall \mathbf{q}_{p-2}\in\mathbf{P}_{p-2}(K),\ \forall \mathbf{v}\in[L^2(K)]^2. \tag{23}$$

Next, for all $\mathbf{u}_n$ and $\mathbf{v}_n$ in $\ker(\widetilde{\mathbf{\Pi}}_p^a)$, define

$$S^K(\mathbf{u}_n,\mathbf{v}_n) = h_K^{-1}\sum_{e\in\mathscr{E}^K}(\widetilde{\mathbf{\Pi}}_{p-1}^{0,e}\mathbf{u}_n, \widetilde{\mathbf{\Pi}}_{p-1}^{0,e}\mathbf{v}_n)_{0,e} + h_K^{-2}(\mathbf{\Pi}_{p-2}^0\mathbf{u}_n, \mathbf{\Pi}_{p-2}^0\mathbf{v}_n)_{0,K}, \tag{24}$$

where $\widetilde{\mathbf{\Pi}}_{p-1}^{0,e}$ and $\mathbf{\Pi}_{p-2}^0$ are defined in (22) and (23), respectively.

In the following result, we prove the two bounds in (19).

Proposition 3.4. *Let $S^K(\cdot,\cdot)$ be the stabilization defined in* (24)*. Then, the bounds in* (19) *are valid with constants c_* and c^* independent of h_K.*

Proof. Let $\mathbf{v}_n\in\ker(\widetilde{\mathbf{\Pi}}_p^a)$. Without loss of generality, we assume $h_K=1$. The assertion follows from a scaling argument.

The bound on c_*. An integration by parts, the definition of the local space $\mathbf{V}_n(K)$ in (10), the Cauchy-Schwarz inequality, and the definition of the stabilization S^K in (24) give

$$\begin{aligned}
a^K(\mathbf{v}_n,\mathbf{v}_n) &= -(\mathbf{v}_n,\mathbf{M}\mathbf{v}_n)_{0,K} + \sum_{e\in\mathscr{E}^K}(\mathbf{v}_n,\gamma_{\mathrm{El}}^K(\mathbf{v}_n))_{0,e}\\
&= -(\mathbf{\Pi}_{p-2}^0\mathbf{v}_n,\mathbf{M}\mathbf{v}_n)_{0,K} + \sum_{e\in\mathscr{E}^K}(\widetilde{\mathbf{\Pi}}_{p-1}^{0,e}\mathbf{v}_n,\gamma_{\mathrm{El}}^K(\mathbf{v}_n))_{0,e}\\
&\le \|\mathbf{\Pi}_{p-2}^0\mathbf{v}_n\|_{0,K}\|\mathbf{M}\mathbf{v}_n\|_{0,K} + \sum_{e\in\mathscr{E}^K}\|\widetilde{\mathbf{\Pi}}_{p-1}^{0,e}\mathbf{v}_n\|_{0,e}\|\gamma_{\mathrm{El}}^K(\mathbf{v}_n)\|_{0,e}\\
&\lesssim S^K(\mathbf{v}_n,\mathbf{v}_n)^{\frac12}\left(\|\mathbf{M}\mathbf{v}_n\|_{0,K}^2 + \sum_{e\in\mathscr{E}^K}\|\gamma_{\mathrm{El}}^K(\mathbf{v}_n)\|_{0,e}^2\right)^{\frac12}.
\end{aligned} \tag{25}$$

We need to prove an upper bound on the second term on the right-hand side in terms of $|\mathbf{v}_n|_{a^K}$. Focus on the bulk term. Using a polynomial inverse inequality on polygons, see, e.g., [7, equation (32)] and [12, Lemma 10], we can write

$$\begin{aligned}\|\mathbf{M}\mathbf{v}_n\|_{0,K} \lesssim \|\mathbf{M}\mathbf{v}_n\|_{-1,K} &:= \sup_{\mathbf{\Phi}\in[H^1_0(K)]^2} \frac{(\mathbf{M}\mathbf{v}_n,\mathbf{\Phi})_{0,K}}{|\mathbf{\Phi}|_{1,K}} \\ &= \sup_{\mathbf{\Phi}\in[H^1_0(K)]^2} \frac{a^K(\mathbf{v}_n,\mathbf{\Phi})}{|\mathbf{\Phi}|_{1,K}} \leq (2\mu+\lambda)|\mathbf{v}_n|_{a^K}.\end{aligned}$$

Eventually, we focus on the boundary terms appearing in the second term on the right-hand side of (25). Using equivalence of (semi)norms in finite dimensional spaces arguing as in [3, Proposition 4.7], we can write

$$\left(\sum_{e\in\mathscr{E}^K} \|\gamma^K_{\mathrm{El}}(\mathbf{v}_n)\|^2_{0,e}\right)^{\frac{1}{2}} \lesssim \|\mu\nabla\mathbf{v}_n + (\mu+\lambda)\mathrm{div}\mathbf{v}_n\|_{0,K} = |\mathbf{v}_n|_{a^K}.$$

The bound on c^*. The second bound is proven using the stability of L^2 projectors in L^2 norms, the fact that functions in $\ker(\widetilde{\mathbf{\Pi}}^a_p)$ have zero average on the boundary, see (17), and the trace and the Poincaré inequalities. □

The discrete right-hand side. The discrete right-hand side is dealt with as in standard virtual elements [6]. Given $\mathscr{V}(K)$ the set of vertices of K, we define

$$\langle \mathbf{f}_n, \mathbf{v}_n\rangle := \begin{cases} \sum_{K\in\mathscr{T}_n} \frac{1}{N^K_V} \sum_{\nu\in\mathscr{V}(K)} (\mathbf{f}, \mathbf{v}_n(\nu))_{0,K} & \text{if } p=1 \\ \sum_{K\in\mathscr{T}_n} (\mathbf{f}, \mathbf{\Pi}^0_{p-2}\mathbf{v}_n)_{0,K} & \text{if } p\geq 2. \end{cases}$$

3.5 The method

We consider the following nonconforming virtual element method:

$$\begin{cases} \text{find } \mathbf{u}_n \in \mathbf{V}_n \text{ such that} \\ a_n(\mathbf{u}_n,\mathbf{v}_n) = \langle \mathbf{f}_n, \mathbf{v}_n\rangle \qquad \forall \mathbf{v}_n \in \mathbf{V}_n. \end{cases} \tag{26}$$

The well posedness of method (26) follows from the Korn's inequality, the Lax-Milgram lemma, and the stability properties of $a_n(\cdot,\cdot)$.

4 Convergence analysis

We present the convergence analysis for method (26) under assumption (7). We follow the lines of the corresponding analysis for the Poisson problem in [3, Section 4]. For the sake of completeness, we provide some details.

After showing abstract error estimates in Section 4.1, we prove upper bounds on all the terms appearing in such estimates; see Sections 4.2, 4.3, and 4.4. In Section 4.5, we state an optimal convergence result.

4.1 Abstract error estimates

We present abstract error estimates for method (26). To the aim, we first introduce a bilinear form $\mathscr{N}_n : [H^{\frac{1}{2}+\varepsilon}(\Omega)]^2 \times [H^{1,nc}_p(\mathscr{T}_n)]^2 \to \mathbb{R}$, $\varepsilon > 0$, representing the variational crime due to the nonconformity of the spaces as follows:

$$\mathscr{N}_n(\mathbf{u},\mathbf{v}_n) := \sum_{K\in\mathscr{T}_n} \int_{\partial K} \gamma^K_{\mathrm{El}}(\mathbf{u})\cdot\mathbf{v}_n = \sum_{e\in\mathscr{E}^I_n} \int_e (\mu\mathscr{E}\mathbf{u} + (\mu+\lambda)\mathrm{div}\mathbf{u})[\![\mathbf{v}_n]\!]. \tag{27}$$

Theorem 4.1. *Let α_* and α^* be the stability constants in* (20)*, and $\mathbf{u}_\pi$ and $\mathbf{u}_I$ be (piecewise) in $\widetilde{\mathbf{P}}_p(K)$ and $\mathbf{V}_n$. Then, given $\mathbf{u}$ and $\mathbf{u}_n$ the solutions to* (3) *and* (26)*, the following a priori estimate is valid:*

$$|\mathbf{u}-\mathbf{u}_n|_{a^{\mathscr{T}_n}} \leq \alpha_*^{-1}\Big\{ (1+\alpha^*)\left(|\mathbf{u}-\mathbf{u}_\pi|_{a^{\mathscr{T}_n}} + |\mathbf{u}-\mathbf{u}_I|_{a^{\mathscr{T}_n}}\right) + \sup_{\mathbf{v}_n\in\mathbf{V}_n} \frac{(\mathbf{f},\mathbf{v}_n)_{0,\Omega} - \langle \mathbf{f}_n,\mathbf{v}_n\rangle}{|\mathbf{v}_n|_{a^{\mathscr{T}_n}}} + \sup_{\mathbf{v}_n\in\mathbf{V}_n} \frac{\mathscr{N}_n(\mathbf{u},\mathbf{v}_n)}{|\mathbf{v}_n|_{a^{\mathscr{T}_n}}} \Big\}.$$

Proof. The proof is fairly standard in the nonconforming VEM literature [3, 4, 26]. Given $\boldsymbol{\delta}_n = \mathbf{u}_n - \mathbf{u}_I \in \mathbf{V}_n$, the triangle inequality implies

$$|\mathbf{u}-\mathbf{u}_n|_{a^{\mathscr{T}_n}} \leq |\mathbf{u}-\mathbf{u}_I|_{a^{\mathscr{T}_n}} + |\boldsymbol{\delta}_n|_{a^{\mathscr{T}_n}}. \tag{28}$$

Consider the second term on the right-hand side. Using (20) and (21), we can write

$$\begin{aligned} |\boldsymbol{\delta}_n|^2_{a^{\mathscr{T}_n}} &= \sum_{K\in\mathscr{T}_n} |\boldsymbol{\delta}_n|^2_{a^K} \leq \alpha_*^{-1} \sum_{K\in\mathscr{T}_n} a_n^K(\boldsymbol{\delta}_n,\boldsymbol{\delta}_n) \\ &= \alpha_*^{-1} \sum_{K\in\mathscr{T}_n} \left(a_n^K(\mathbf{u}_n,\boldsymbol{\delta}_n) - a_n^K(\mathbf{u}_I-\mathbf{u}_\pi,\boldsymbol{\delta}_n) - a^K(\mathbf{u}_\pi-\mathbf{u},\boldsymbol{\delta}_n) - a^K(\mathbf{u},\boldsymbol{\delta}_n)\right). \end{aligned}$$

An integration by parts and (27) entail

$$\sum_{K\in\mathscr{T}_n} a^K(\mathbf{u},\boldsymbol{\delta}_n) = (\mathbf{f},\boldsymbol{\delta}_n)_{0,\Omega} + \mathscr{N}_n(\mathbf{u},\boldsymbol{\delta}_n).$$

Using again (20), (28), and standard manipulations give the assertion. □

4.2 Best enriched polynomial and virtual interpolation estimates

We review certain enriched polynomial and interpolation estimates. We follow the lines of [3, Sections 4.2 and 4.3]. We begin with stating a best enriched polynomial estimate. Its proof is the vector version of [3, Lemma 4.2] and is therefore omitted.

Lemma 4.2. *Given $\mathbf{u}$ the solution to* (3) *and $\mathbf{u}_0$ its smooth part as in* (7)*, there exists $\mathbf{u}_\pi$ piecewise in $\widetilde{\mathbf{P}}_p(K)$ such that*

$$|\mathbf{u}-\mathbf{u}_\pi|_{a^{\mathscr{T}_n}} \lesssim h^p \Big\{ \Big(\sum_{K\in\mathscr{T}_n^1} |\mathbf{u}_0|^2_{p+1,K} \Big)^{\frac{1}{2}} + \Big(\sum_{K\in\mathscr{T}_n^2\cup\mathscr{T}_n^3} |\mathbf{u}|^2_{p+1,K} \Big)^{\frac{1}{2}} \Big\}.$$

We conclude the section by proving interpolation estimates, which are a consequence of Proposition 3.2 and Lemma 4.2.

Lemma 4.3. *Given $\mathbf{u}$ the solution to* (3) *and $\mathbf{u}_0$ its smooth part as in* (7)*, there exists $\mathbf{u}_I$ in $\mathbf{V}_n$ such that*

$$|\mathbf{u}-\mathbf{u}_I|_{a^{\mathscr{T}_n}} \lesssim h^p \Big\{ \Big(\sum_{K\in\mathscr{T}_n^1} |\mathbf{u}_0|^2_{p+1,K} \Big)^{\frac{1}{2}} + \Big(\sum_{K\in\mathscr{T}_n^2\cup\mathscr{T}_n^3} |\mathbf{u}|^2_{p+1,K} \Big)^{\frac{1}{2}} \Big\}.$$

In words, even if the solution $\mathbf{u}$ of (3) is singular, approximation and interpolation estimates by means of enriched polynomials and enriched virtual element functions are optimal with respect to the polynomial degree of accuracy of the method.

4.3 Approximation of the right-hand side

We show an upper bound on the term representing the variational crime on the right-hand side, i.e.,

$$\sup_{\mathbf{v}_n\in\mathbf{V}_n} \frac{(\mathbf{f},\mathbf{v}_n)_{0,\Omega} - \langle \mathbf{f}_n,\mathbf{v}_n\rangle}{|\mathbf{v}_n|_{a^{\mathscr{T}_n}}}.$$

No enrichment is used in the discretization of the right-hand side. Thus, the following bound follows as in standard virtual elements [6].

Lemma 4.4. *Given* $\mathbf{f} \in H^{p-1}(\Omega)$ *the right-hand side of* (3)*, the following bound is valid:*

$$\sup_{\mathbf{v}_n \in \mathbf{V}_n} \frac{(\mathbf{f}, \mathbf{v}_n)_{0,\Omega} - \langle \mathbf{f}_n, \mathbf{v}_n \rangle}{|\mathbf{v}_n|_{a^{\mathscr{T}_n}}} \lesssim h^p \|\mathbf{f}\|_{p-1,\Omega}.$$

4.4 Approximation of the nonconformity term

Recall that $\mathscr{N}_n(\cdot,\cdot)$ is defined in (27). We show an upper bound on the term representing the variational crime due to the nonconformity of the method, i.e.,

$$\sup_{\mathbf{v}_n \in \mathbf{V}_n} \frac{\mathscr{N}_n(\mathbf{u}, \mathbf{v}_n)}{|\mathbf{v}_n|_{a^{\mathscr{T}_n}}}.$$

Lemma 4.5. *Given* $\mathbf{u}$ *the solution to* (3)*,* $\mathbf{u}_0$ *as in* (7)*, and* $\mathscr{N}_n(\cdot,\cdot)$ *as in* (27)*. Then, the following bound is valid:*

$$\sup_{\mathbf{v}_n \in \mathbf{V}_n} \frac{\mathscr{N}_n(\mathbf{u}, \mathbf{v}_n)}{|\mathbf{v}_n|_{a^{\mathscr{T}_n}}} \lesssim h^p \Big\{ \Big(\sum_{K \in \mathscr{T}_n^1} |\mathbf{u}_0|_{p+1,K}^2 \Big)^{\frac{1}{2}} + \Big(\sum_{K \in \mathscr{T}_n^2 \cup \mathscr{T}_n^3} |\mathbf{u}|_{p+1,K}^2 \Big)^{\frac{1}{2}} \Big\}.$$

Proof. The proof follows along the same lines as that of [3, Lemma 4.6]. For the sake of clarity, we report some details. Since $\mathscr{N}_n(\cdot,\cdot)$ is defined as a sum over all internal edges, we fix e in $\mathscr{E}_n^I$.

Given e in $\mathscr{E}_n^I$, we introduce K^+ and K^- such that

$$\overline{K^+} \cap \overline{K^-} \supset e, \qquad \mathbf{n}_{K^+} \cdot \mathbf{n}_e = 1, \qquad \mathbf{n}_{K^-} \cdot \mathbf{n}_e = -1.$$

Using the definition of nonconforming functions (15), we can write

$$\begin{aligned}\int_e (\mu \mathscr{E}\mathbf{u} + (\mu+\lambda)\mathrm{div}\mathbf{u})[\![\mathbf{v}]\!] &= \int_e \gamma_{\mathrm{El}}^e(\mathbf{u}) \cdot (\mathbf{v}_{n|K^+} - \mathbf{v}_{n|K^-}) = \int_e \gamma_{\mathrm{El}}^e(\mathbf{u}_0) \cdot (\mathbf{v}_{n|K^+} - \mathbf{v}_{n|K^-}) \\ &\le \|\gamma_{\mathrm{El}}^e(\mathbf{u}_0) - \widetilde{\mathbf{\Pi}}_{p-1}^{0,e} \gamma_{\mathrm{El}}^e(\mathbf{u}_0)\|_{0,e} \|\mathbf{v}_{n|K^+} - \mathbf{v}_{n|K^-} - \widetilde{\mathbf{\Pi}}_{p-1}^{0,e}(\mathbf{v}_{n|K^+} - \mathbf{v}_{n|K^-})\|_{0,e}.\end{aligned}$$

Given K either K^+ or K^-, introduce $\mathbf{\Pi}_p^\nabla : [H^1(K)]^2 \to \mathbf{P}_p(K)$ any $H^1(K)$ projector onto standard polynomials. Using the properties of orthogonal projectors, a trace inequality, and the Poincaré-Wirtinger inequality, we arrive at

$$\int_e (\mu \mathscr{E}\mathbf{u} + (\mu+\lambda)\mathrm{div}\mathbf{u})[\![\mathbf{v}]\!] \lesssim h_K^{\frac{1}{2}} |\mathbf{u}_0 - \mathbf{\Pi}_p^\nabla \mathbf{u}_0|_{1,K} h_K^{\frac{1}{2}} \left(|\mathbf{v}_n|_{a^{K^+}}^2 + |\mathbf{v}_n|_{a^{K^-}}^2 \right)^{\frac{1}{2}}.$$

The assertion follows from standard polynomial approximation estimates and the smoothness of $\mathbf{u}_0$. □

4.5 Convergence estimate

We collect the foregoing estimates and exhibit the optimal convergence rate for method (26).

Theorem 4.6. *Let* $\mathbf{u}$ *and* $\mathbf{u}_n$ *be the solutions to* (3) *and* (26) *with right-hand side* $\mathbf{f} \in H^{p-1}(\Omega)$*, and* $\mathbf{u}_0$ *as in* (7)*. Then, the exists a positive constant* c *depending on* α_* *and* α^* *in* (20) *such that*

$$|\mathbf{u} - \mathbf{u}_n|_{a^{\mathscr{T}_n}} \lesssim h^p \Big\{ \Big(\sum_{K \in \mathscr{T}_n^1} |\mathbf{u}_0|_{p+1,K}^2 \Big)^{\frac{1}{2}} + \Big(\sum_{K \in \mathscr{T}_n^2 \cup \mathscr{T}_n^3} |\mathbf{u}|_{p+1,K}^2 \Big)^{\frac{1}{2}} + \|\mathbf{f}\|_{p-1,\Omega} \Big\}.$$

Proof. The assertion follows combining Theorem 4.1, and Lemmas 4.2, 4.3, 4.4, and 4.5. □

5 Numerical experiments

We investigate numerically the convergence rate of method (26) from Theorem 4.6. The numerical assessment of accuracy and convergence is processed in relation to the relevant singularity patterns and mechanical interpretation emerging in each problem.

Throughout the numerical campaign, we shall refer to: standard, partially enriched, and fully enriched versions of method (26). The first one corresponds to the standard nonconforming virtual element method; the second one to the method with enrichment on few elements close to the "singular" vertices as detailed in Section 3.1 (we henceforth take $\gamma = 0.1$); the third one to the method with enrichment on all elements.

As the discrete solution $\mathbf{u}_n$ to (26) is not available in closed form, we employ the following computable error measure:

$$\frac{\left|\mathbf{u} - \mathbf{\Pi}_p^{\nabla} \mathbf{u}_n\right|_{a^{\mathscr{T}_n}}}{|\mathbf{u}|_{1,\Omega}}.$$

With an abuse of notation, we shall refer to the above quantity as the H^1 *error*.

Following [3], we orthogonalize the enriched polynomial basis functions on each edge used in the definition of the edge degrees of freedom (12)–(13). This is a beneficial procedure in improving the condition number of the stiffness matrix, which can be performed due to the nonconforming structure of the discrete spaces.

This section is organized as follows. In Sections 5.1 and 5.2, we assess method (26) on the two benchmarks detailed in Examples A.1 and A.2 below; in Section 5.3, we discuss possible extensions and comparison with other methods.

5.1 L-shaped domain

We consider singular solutions on the L-shaped domain aiming at confirming the accuracy and efficiency of method (26) on a pure mathematical benchmark and assessing sensitivity to degree elevation.

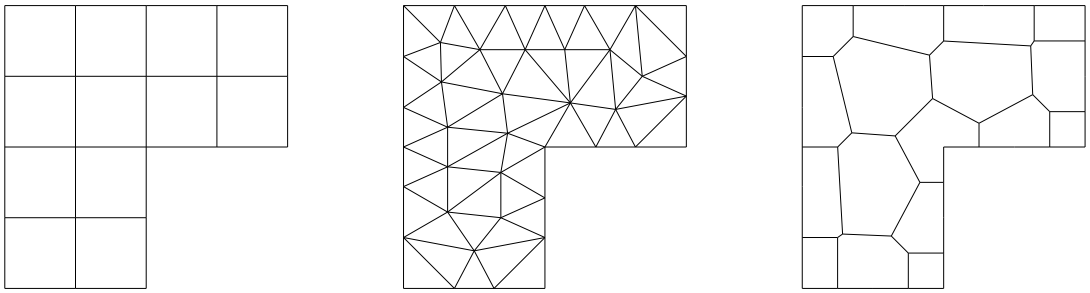

Figure 4: Types of meshes employed on the L-shaped domain: uniform Cartesian (*left panel*); random triangles (*central panel*); Voronoi polygons (*right panel*).

5.1.1 Increasing the polynomial degree of accuracy

We measure the method sensitivity to the polynomial degree of accuracy p elevation according to the singular patch test derived in Section A.1 below, i.e., for the exact solution in (36) given by

$$\mathbf{u}_1(r,\theta) = r^{\frac{7}{6}} \mathscr{S}_{\mathbf{A}}(\theta). \tag{29}$$

Homogeneous Dirichlet (clamped) boundary conditions are fixed along the edges at the re-entrant corner. This test case is considered with the aim of checking the consistency of the method with respect to singular functions.

We pick a uniform Cartesian mesh with mesh size $h = 1/4$, see Figure 4 (*left panel*), and in Figure 5 plot the H^1-error for polynomial degree of accuracy p ranging from 1 to 8. We only consider the fully enriched version of the method.

Since the exact solution belongs to the global virtual element space and the method is consistent with respect to polynomials and singular functions, we expect the error to be zero up to machine precision. This is what we observe in Figure 5. The error grows with the condition number of the stiffness matrix. In turns, the condition number increases with p as standard in the p-version of any Galerkin method. A further reduction of such an ill-conditioning would be possible by performing

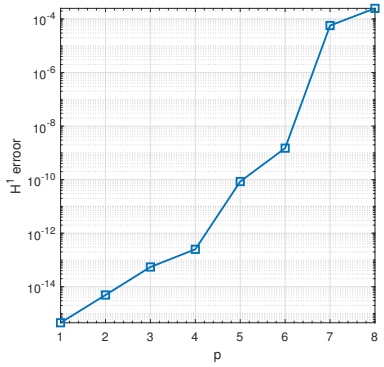

Figure 5: Singular patch test $\mathbf{u}_1$ defined in (29) on the L-shaped domain. p-version of the fully enriched version of method (26). We fix a uniform Cartesian mesh with size $= 1/4$; see Figure 4 (*left panel*).

an extra orthogonalization of the polynomial basis elements employed in the definition of the bulk degrees of freedom (11) as in [25].

5.1.2 Convergence under uniform mesh refinements

Given $\mathbf{u}_1$ as in (29), we investigate the equilibrium problem on the L-shaped domain for the exact solution

$$\mathbf{u}_2(x, y) = \mathbf{u}_2(r, \theta) = (\sin(\pi x)\sin(\pi y); \sin(\pi x)\sin(\pi y))^T + \mathbf{u}_1(r, \theta). \tag{30}$$

Homogeneous Dirichlet (clamped) boundary conditions are still fixed at the re-entrant corner edges. Sequences of uniform Cartesian, random triangles, and Voronoi polygonal meshes are used; see Figure 4 for a representation of the coarsest mesh of each type.

We present numerical results for the standard, partially enriched ($\gamma = 0.1$), and fully enriched h-version of the method with polynomial degree of accuracy $p = 1$, 2, and 3; see Figure 6 and Table 2.

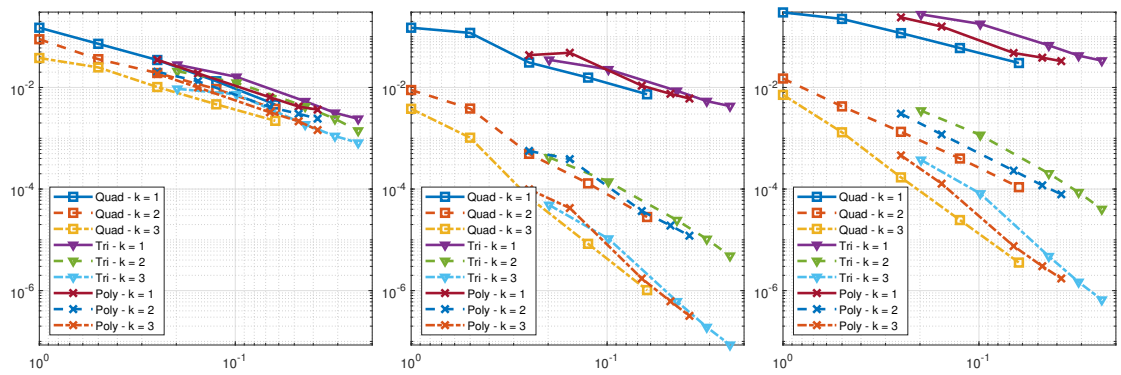

Figure 6: Singular solution $\mathbf{u}_2$ defined in (30) on the L-shaped domain. Standard (*left panel*), partially enriched with $\gamma = 0.1$ (*central panel*), and fully enriched (*right panel*) h-versions of method (26). Degrees of accuracy $p = 1$ (solid), 2 (dashed), and 3 (dash-dotted). Sequences of uniform Cartesian (Quad), random triangle (Tri), and Voronoi polygon (Poly) meshes, as in Figure 4.

Table 2 Orders of convergence corresponding to each mesh refinement from Figure 6 for the exact solution $\mathbf{u}_2$ in (30).

	standard method								
	QUAD			TRI			POLY		
	$k=1$	$k=2$	$k=3$	$k=1$	$k=2$	$k=3$	$k=1$	$k=2$	$k=3$
mesh ref. #1	1.0512	1.3042	0.6149	0.7901	0.7537	0.3613	1.2880	0.9002	1.2899
mesh ref. #2	1.0598	0.9036	1.2831	1.3734	1.3319	1.6941	1.2827	1.3849	1.3311
mesh ref. #3	1.3891	1.0512	1.1307	1.4956	1.6056	1.4991	1.2494	0.8994	1.2107
mesh ref. #4	1.5190	1.2954	1.0784	0.9943	1.9566	1.1138	0.6191	0.9802	1.7720
	partially enriched method								
	QUAD			TRI			POLY		
	$k=1$	$k=2$	$k=3$	$k=1$	$k=2$	$k=3$	$k=1$	$k=2$	$k=3$
mesh ref. #1	0.3370	1.2115	1.8896	0.6234	1.5871	2.1946	-0.2259	0.7741	1.7741
mesh ref. #2	1.9405	2.9610	3.9135	1.2067	2.1652	3.5275	1.7639	2.7821	3.7760
mesh ref. #3	0.9844	1.9321	3.0274	1.3289	2.4390	3.3324	1.0974	1.9569	3.0695
mesh ref. #4	1.0904	2.2009	3.0291	0.8276	2.7899	2.9471	0.9588	2.0616	2.9525
	fully enriched method								
	QUAD			TRI			POLY		
	$k=1$	$k=2$	$k=3$	$k=1$	$k=2$	$k=3$	$k=1$	$k=2$	$k=3$
mesh ref. #1	0.4231	1.8227	2.4482	0.6234	1.5871	2.1946	0.8721	1.9684	2.6809
mesh ref. #2	0.9292	1.6627	2.9484	1.2067	2.1652	3.5275	1.4167	1.9410	3.3470
mesh ref. #3	0.9772	1.7462	2.7914	1.3289	2.4390	3.3324	0.6276	1.9765	2.7067
mesh ref. #4	0.9775	1.8752	2.7820	0.8276	2.7899	2.9471	0.7088	1.8292	2.4894

The standard nonconforming VEM suffers from a lack of accuracy due to intrinsic inconsistency with the problem solution: the rate of convergence is suboptimal compared to the polynomial degree of accuracy. Instead, the two enriched version converge with (optimal) order p.

The partially enriched version offers the most effective option in terms of accuracy, conditioning, and computational cost, leading to optimal rate of convergence and error levels with respect to the more cumbersome fully enriched version.

5.2 Slit domain

We assess numerically the equilibrium of the bi-unit slit domain with homogeneous Neumann boundary conditions along the edges emanating from the internal corner: this is the actual configuration at the crack apex for a material with zero cohesion and no friction. The problem setup is discussed in Example A.2 below; there, we derive the corresponding two strongest singular terms appearing in the expansion at the crack tip, for the given geometry and boundary conditions; see also [28].

In particular, given $\mathscr{S}^1_{\mathbf{A}}(\theta)$ and $\mathscr{S}^2_{\mathbf{A}}(\theta)$ as in (38) and (39), we consider the exact solution

$$\mathbf{u}_3(x,y) = \mathbf{u}_3(r,\theta) = (\sin(\pi x)\sin(\pi y); \sin(\pi x)\sin(\pi y))^T + r^{\frac{1}{2}}\mathscr{S}^1_{\mathbf{A}}(\theta) + r^{\frac{1}{2}}\mathscr{S}^2_{\mathbf{A}}(\theta). \tag{31}$$

We employ sequences of Quad, Tri, and Voro meshes as in Figure 7, and polynomial degree of accuracy $p = 1$, 2, and 3. Standard, partially enriched ($\gamma = 0.1$), and fully enriched versions of the method are explored. We report the numerical results in Figure 8 and Table 3.

An inspection of Figure 8 and Table 3 reveals optimal convergence rates for the partially and fully enriched versions of the method, still with an edge in favour of the former, which is the less computationally expensive and less ill-conditioned. The standard version remains suboptimal in the polynomial degree of accuracy.

5.3 Extensions and comparison with other methods

Method (26) can be extended so as to approximate solutions to other relevant engineering problems as those in, e.g., [1, 2, 10, 21, 29].

Compared to extended Galerkin methods as in [9, 28], the present approach yields better conditioned linear systems, thanks to orthogonalization strategies of enriched polynomial spaces as in [3], which would yield loss of sparsity of the stiffness matrix in the conforming setting.

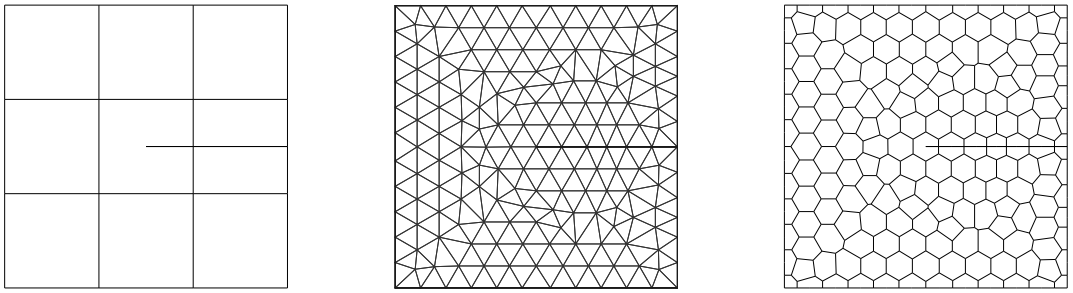

Figure 7: Slit domain mesh types: uniform Cartesian (*left panel*); random triangles (*central panel*); Voronoi polygons (*right panel*).

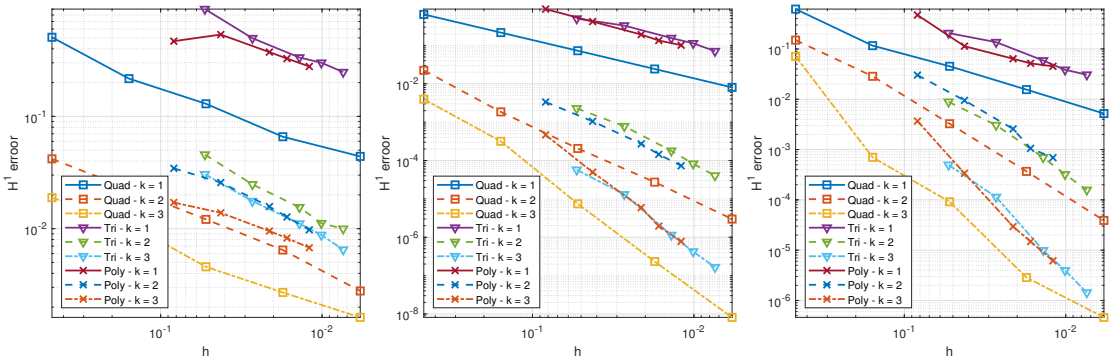

Figure 8: Singular solution $\mathbf{u}_3$ defined in (31) on the slit domain. Standard (*left panel*), partially enriched with $\gamma = 0.1$ (*central panel*), and fully enriched (*right panel*) h-versions of method (26). Degrees of accuracy $p = 1$ (solid), 2 (dashed), and 3 (dash-dotted). Sequences of uniform Cartesian (Quad), random triangle (Tri), and Voronoi polygon (Poly) meshes, as in Figure 7.

In fact, in partition of unity based Galerkin methods the inclusion of singular functions in the discrete space is performed by multiplying the singular functions with the usual hat functions, which form a partition of unity. Notably, the support of the resulting function is the patch of elements sharing a vertex. Any orthogonalization procedure (for instance a stable Gram-Schmidt process) of the resulting basis functions would lead to basis functions with support given by the (increasing) union of vertex patches.

On the other hand, the orthogonalization procedure employed in the ncVEM, see [3] instead leads to "orthogonalized" basis functions with the same support of the original basis: edge basis functions have support given by the union of the elements sharing the given edge; bulk basis functions have support given by a single element.

6 Conclusions

We introduced a novel nonconforming virtual element method with discrete spaces enriched with suitable singular functions for the approximation of solutions to the isotropic linear elasticity problem. The proposed methodology offers a viable and efficient strategy of accurately modeling the cracking phenomenon of linear elastic material bodies with no dependence on the material parameters of the fracturing medium. The natural inclusion of the analytical singularities offered by the presented approach makes it an interesting candidate for the development of nonlinear crack tracking procedures purely based on fracture mechanics.

Table 3 Orders of convergence corresponding to each mesh refinement from Figure 6 for the exact solution $\mathbf{u}_2$ in (30).

	standard method								
	QUAD			TRI			POLY		
	$k=1$	$k=2$	$k=3$	$k=1$	$k=2$	$k=3$	$k=1$	$k=2$	$k=3$
mesh ref. #1	0.7720	0.5628	0.4929	0.8802	0.9010	0.8116	-0.2022	0.4342	0.3160
mesh ref. #2	0.4698	0.5675	0.7980	0.5903	0.6990	0.6865	0.5190	0.7121	0.5392
mesh ref. #3	0.6161	0.5730	0.4806	0.3437	1.0477	0.7493	0.5265	0.8472	0.5739
mesh ref. #4	0.3652	0.7605	0.4627	0.6169	0.3666	0.9675	0.5105	0.8309	0.6227
	partially enriched method								
	QUAD			TRI			POLY		
	$k=1$	$k=2$	$k=3$	$k=1$	$k=2$	$k=3$	$k=1$	$k=2$	$k=3$
mesh ref. #1	0.9943	2.2687	2.2995	0.6132	1.5758	2.1727	1.1194	1.7281	3.3404
mesh ref. #2	0.9917	1.9996	3.4185	1.1193	2.1990	3.6351	1.1255	1.9527	3.0675
mesh ref. #3	0.9996	1.8413	3.1572	1.0053	2.4939	3.1818	1.4204	2.5217	4.4240
mesh ref. #4	1.0002	2.0083	3.0366	1.5171	2.2800	3.0270	0.8787	2.1447	2.8780
	fully enriched method								
	QUAD			TRI			POLY		
	$k=1$	$k=2$	$k=3$	$k=1$	$k=2$	$k=3$	$k=1$	$k=2$	$k=3$
mesh ref. #1	1.5236	1.5074	4.2058	0.6132	1.5758	2.1727	2.1242	1.7281	3.5660
mesh ref. #2	0.8596	1.9762	1.8529	1.2489	2.1990	3.6351	0.8301	1.8845	3.5146
mesh ref. #3	0.9743	1.9906	3.1613	1.3701	2.4939	2.9431	0.8521	3.5568	2.7452
mesh ref. #4	0.9917	2.0329	1.6528	0.7175	2.2800	3.2665	0.4202	1.3280	2.7661

A On some corner singularities for the isotropic linear elasticity problem on polygons

Recall splitting (4) and denote the measure of the angle at $\mathbf{A}$ by ω. In the following, we review the behaviour of the singular components $\mathscr{S}_{\mathbf{A}}$ in the neighbourhood of vertex $\mathbf{A}$ of Ω. Such singular functions are typically given by the sum of several singular terms. In Section A.1, we focus on each single term of such expansion on a couple of benchmark domains; notably, we exhibit possible choices of such terms. Instead, in Section A.2, we review the full singular expansion.

A.1 Singular functions at corners

We compute explicitly singular solutions at corners in the kernel of the operator $\mathbf{M}$ defined in (1) of the form (5). These solutions represents singular displacement fields, corresponding to self-equilibrated stress states for the 2D material body exhibiting a re-entrant corner, which tend to infinity at the tip of the corner. Notably, the parameter α, and the functions $\mathscr{S}_1$ and $\mathscr{S}_2$ in (5) are computed in a two step procedure:

- impose the constraint
$$\mathbf{M}(r^\alpha(\mathscr{S}_1(\theta),\mathscr{S}_2(\theta))^T)=\mathbf{0} \qquad \text{in } \Omega; \tag{32}$$
- impose the boundary conditions for $\theta=0$ and $\theta=\omega$.

Introduce
$$F(\alpha):=\lambda+3\mu-\alpha(\lambda+\mu), \qquad G(\alpha):=\lambda+3\mu+\alpha(\lambda+\mu).$$
As in [30, equation (4.7)], imposing (32) for functions in the form (5) yields, for $\alpha\in\mathbb{R}^+$ to be fixed later,
$$\begin{aligned}\mathscr{S}_{\mathbf{A}}(\theta)=c_1(\alpha)\begin{pmatrix}\cos[(1+\alpha)\theta]\\-\sin[(1+\alpha)\theta]\end{pmatrix}+c_2(\alpha)\begin{pmatrix}\sin[(1+\alpha)\theta]\\\cos[(1+\alpha)\theta]\end{pmatrix}\\+c_3(\alpha)\begin{pmatrix}F(\alpha)\cos[(1-\alpha)\theta]\\-G(\alpha)\sin[(1-\alpha)\theta]\end{pmatrix}+c_4(\alpha)\begin{pmatrix}F(\alpha)\sin[(1-\alpha)\theta]\\G(\alpha)\cos[(1-\alpha)\theta]\end{pmatrix}.\end{aligned} \tag{33}$$
So far, α denotes an arbitrary singular exponents at corner $\mathbf{A}$, which has to be fixed so that the function in (33) fulfils suitable homogeneous boundary conditions. Explicit choices of α are

determined solving a 4×4 system with unknowns given by $c_j(\alpha)$, $j = 1, \dots, 4$, which is obtained imposing the homogeneous boundary conditions.

Recall that ω denotes the measure of $\mathbf{A}$ and that the angular part of the polar coordinates takes value in $(0, \omega)$. For the sake of exposition, we focus on Dirichlet boundary conditions only, which correspond to *clamped edges* of the re-entrant corner.

Imposing homogeneous Dirichlet boundary conditions in (33), the resulting 4×4 system reads

$$\begin{pmatrix} \cos[(1+\alpha)0] & \sin[(1+\alpha)0] & F(\alpha)\cos[(1-\alpha)0] & F(\alpha)\sin[(1-\alpha)0] \\ \cos[(1+\alpha)\omega] & \sin[(1+\alpha)\omega] & F(\alpha)\cos[(1-\alpha)\omega] & F(\alpha)\sin[(1-\alpha)\omega] \\ -\sin[(1+\alpha)0] & \cos[(1+\alpha)0] & -G(\alpha)\sin[(1-\alpha)0] & G(\alpha)\cos[(1-\alpha)0] \\ -\sin[(1+\alpha)\omega] & \cos[(1+\alpha)\omega] & -G(\alpha)\sin[(1-\alpha)\omega] & G(\alpha)\cos[(1-\alpha)\omega] \end{pmatrix} \begin{pmatrix} c_1(\alpha) \\ c_2(\alpha) \\ c_3(\alpha) \\ c_4(\alpha) \end{pmatrix} = \begin{pmatrix} 0 \\ 0 \\ 0 \\ 0 \end{pmatrix},$$

i.e.,

$$\begin{pmatrix} 1 & 0 & F(\alpha) & 0 \\ \cos[(1+\alpha)\omega] & \sin[(1+\alpha)\omega] & F(\alpha)\cos[(1-\alpha)\omega] & F(\alpha)\sin[(1-\alpha)\omega] \\ 0 & 1 & 0 & G(\alpha) \\ -\sin[(1+\alpha)\omega] & \cos[(1+\alpha)\omega] & -G(\alpha)\sin[(1-\alpha)\omega] & G(\alpha)\cos[(1-\alpha)\omega] \end{pmatrix} \begin{pmatrix} c_1(\alpha) \\ c_2(\alpha) \\ c_3(\alpha) \\ c_4(\alpha) \end{pmatrix} = \begin{pmatrix} 0 \\ 0 \\ 0 \\ 0 \end{pmatrix}. \quad (34)$$

System (34) admits a nontrivial solution if the determinant of the system matrix is zero. Imposing such a determinant to be zero is equivalent to solving the so-called *characteristic equation*.

In the case of homogeneous Dirichlet, i.e., clamped boundary conditions, the characteristic equation reads as follows, see, e.g., [30, Section 4] [1] find $\alpha \in \mathbb{R}_+$ such that

$$\sin^2(\alpha\omega) - \alpha^2 \lambda \frac{\lambda + 2\mu}{(\lambda + 3\mu)^2} \sin^2 \omega = 0. \quad (35)$$

Next, we look for explicit α solutions to (35) on two benchmark domains.

Example A.1. We focus on the re-entrant corner $(0, 0)$ of the L-shaped domain

$$\Omega_1 := (-1, 1)^2 \setminus [0, 1) \times (-1, 0],$$

and fix the following Lamé parameters:

$$\lambda = -\frac{7}{2} + 9\frac{\sqrt{2}}{2}, \qquad \mu = \frac{7}{2} - 3\frac{\sqrt{2}}{2}.$$

We have $\omega = 3\pi/2$; the first three real smallest solutions to (35) read

$$\alpha_1 = 0.58917798046021; \qquad \alpha_2 = 0.769651906609214; \qquad \alpha_3 = 7/6.$$

The corresponding characteristic equation has a finite number of real solutions.

Next, we show how to recover the singular function in (5). To the aim, we only consider the case $\alpha = \alpha_3$. The coefficients $c_j(7/6)$, $j = 1, \dots, 4$, in (33) are found by solving the system (34) for the given values of α, λ, and μ. In particular, the rank-3 system is

$$\begin{pmatrix} 1 & 0 & 7\left(1 - \frac{\sqrt{2}}{2}\right) & 0 \\ -\frac{\sqrt{2}}{2} & -\frac{\sqrt{2}}{2} & 7\left(1 - \frac{\sqrt{2}}{2}\right)\frac{\sqrt{2}}{2} & -7\left(1 - \frac{\sqrt{2}}{2}\right)\frac{\sqrt{2}}{2} \\ 0 & 1 & 0 & 7\left(1 + \frac{\sqrt{2}}{2}\right) \\ \frac{\sqrt{2}}{2} & -\frac{\sqrt{2}}{2} & 7\left(1 + \frac{\sqrt{2}}{2}\right)\frac{\sqrt{2}}{2} & 7\left(1 + \frac{\sqrt{2}}{2}\right)\frac{\sqrt{2}}{2} \end{pmatrix} \begin{pmatrix} c_1(7/6) \\ c_2(7/6) \\ c_3(7/6) \\ c_4(7/6) \end{pmatrix} = \begin{pmatrix} 0 \\ 0 \\ 0 \\ 0 \end{pmatrix}.$$

There are infinite solutions to this problem: for any $c_4(7/6)$,

$$c_1(7/6) = 7\left(1 - \frac{\sqrt{2}}{2}\right)(\sqrt{2} + 1)c_4(7/6), \qquad c_2(7/6) = -7\left(1 + \frac{\sqrt{2}}{2}\right)c_4(7/6),$$
$$c_3(7/6) = -(\sqrt{2} + 1)c_4(7/6).$$

[1] In [30, (4.11)], the corresponding characteristic equation reads as follows:

$$\sin^2(\alpha\omega) - \alpha^2 \left(\frac{\lambda + \mu}{\lambda + 3\mu}\right)^2 \sin^2 \omega = 0.$$

The reason for this is that the angle at the vertex is $(0, \omega)$ in our setting; $(-\omega/2, \omega/2)$ in [30].

In particular, the explicit singular solution belongs to $H^{\frac{13}{6}-\varepsilon}(\Omega)$, for all arbitrarily small, positive ε, and is a multiple of

$$r^{\frac{7}{6}}\mathscr{S}_{\mathbf{A}}(\theta) = r^{\frac{7}{6}}\left[7(1-\sqrt{2}/2)(\sqrt{2}+1)\begin{pmatrix}\cos(13\theta/6)\\ -\sin(13\theta/6)\end{pmatrix} - 7(1+\sqrt{2}/2)\begin{pmatrix}\sin(13\theta/6)\\ \cos(13\theta/6)\end{pmatrix}\right.$$
$$\left. -(\sqrt{2}+1)\begin{pmatrix}7\left(1-\frac{\sqrt{2}}{2}\right)\cos(\theta/6)\\ +7\left(1+\frac{\sqrt{2}}{2}\right)\sin(\theta/6)\end{pmatrix} + \begin{pmatrix}-7\left(1-\frac{\sqrt{2}}{2}\right)\sin(\theta/6)\\ 7\left(1+\frac{\sqrt{2}}{2}\right)\cos(\theta/6)\end{pmatrix}\right]. \tag{36}$$

Example A.2. We focus on the tip of the the slit domain

$$\Omega_2 := (-1,-1)^2 \setminus \{\{0\}\times[0,1)\}.$$

In this case, $\omega = 2\pi$ and (35) simply reads

$$\sin^2(2\pi\alpha) = 0.$$

This equation has positive solutions α given by

$$2\pi\alpha = k\pi \quad \forall k\in\mathbb{N} \qquad \longrightarrow \alpha = \frac{k}{2} \quad \forall k\in\mathbb{N}.$$

Interestingly, all the singular values α do not depend on the Lamé coefficients.

For the sake of exposition, we focus on the strongest singularity $\alpha = 1/2$. Compute

$$F(1/2) = \frac{1}{2}\lambda + \frac{5}{2}\mu, \qquad G(1/2) = \frac{3}{2}\lambda + \frac{7}{2}\mu.$$

The coefficients $c_j(\alpha)$, $j = 1,\dots,4$, in (33) are found by solving the system (34) for the given α, and for all λ and μ. In particular, the rank-2 system is

$$\begin{pmatrix}1 & 0 & F(1/2) & 0\\ -1 & 0 & -F(1/2) & 0\\ 0 & 1 & 0 & G(1/2)\\ 0 & -1 & 0 & -G(1/2)\end{pmatrix}\begin{pmatrix}c_1(1/2)\\ c_2(1/2)\\ c_3(1/2)\\ c_4(1/2)\end{pmatrix} = \begin{pmatrix}0\\0\\0\\0\end{pmatrix}. \tag{37}$$

There are two families of solutions to the linear system (34). They correspond to the two following choices of the coefficients in (33):

$$c_1(1/2) = -F(1/2)c_3(1/2) \qquad \forall c_3(1/2)\in\mathbb{R}, \qquad c_2(1/2) = -G(1/2)c_3(1/2) \qquad \forall c_4(1/2)\in\mathbb{R}.$$

Thus, the singular solutions are

$$r^{\frac{1}{2}}\mathscr{S}^1_{\mathbf{A}}(\theta) = r^{\frac{1}{2}}\left[-F(1/2)\begin{pmatrix}\cos(3/2\theta)\\ -\sin(3/2\theta)\end{pmatrix} + \begin{pmatrix}F(1/2)\sin(1/2\theta)\\ -G(1/2)\cos(1/2\theta)\end{pmatrix}\right] \tag{38}$$

and

$$r^{\frac{1}{2}}\mathscr{S}^2_{\mathbf{A}}(\theta) = r^{\frac{1}{2}}\left[-G(1/2)\begin{pmatrix}\sin(3/2\theta)\\ \cos(3/2\theta)\end{pmatrix} + \begin{pmatrix}F(1/2)\sin(1/2\theta)\\ G(1/2)\cos(1/2\theta)\end{pmatrix}\right]. \tag{39}$$

The functions in (38) and (39) belong to $H^{\frac{3}{2}-\varepsilon}(\Omega)$, for all arbitrarily small, positive ε. They are found in linear elastic fracture mechanics as reported, e.g., in the classical paper [28].

The Lamé parameters do not come into play in the singular exponents α, but only in the linear combination appearing in the above singular functions. This is not the case of Example A.1, where also the singular exponent α used to depend on the Lamé parameters.

Besides, there are infinitely many singular exponents α. Instead, in Example A.1, there is only a finite number of real exponents α.

Remark 1. So far, we mainly focused on the case of Dirichlet and homogeneous Neumann boundary conditions on the two edges abutting vertex **A**. The above way of reasoning extends to all possible combinations of boundary conditions. We refer to [30] for the counterpart of the characteristic equation to solve. The relevant point is that, in the analysis of the method, the actual representation of the singular function is not relevant as long as it satisfies (6).

A.2 General singular expansions at vertices

We review the full singular expansions at a vertex as in [30]; see also [16, 20, 27].

Let α_0 be such that (32) is satisfied and let $\mathbf{e}_0 = \mathbf{e}_0(\alpha, \varphi)$ be an associated eigenfunction. The set of fields $\{\mathbf{e}_{0,0}, \mathbf{e}_{0,1}, \ldots, \mathbf{e}_{0,k}\}$ with $\mathbf{e}_{0,0} = \mathbf{e}_0$ is called a Jordan chain to α if

$$\sum_{q=0}^{m} \frac{1}{m!} \left(\frac{\partial}{\partial \alpha}\right)^q \mathbf{M}\, \mathbf{e}_{0,m-q}(\alpha, \theta)_{|\alpha=\alpha_0} = 0 \qquad \forall m = 1, 2, \ldots, k.$$

We call the number $k+1$ the *length of the Jordan chain*.

The main result of this section was proven, e.g., in [30, Theorem 3.1]; see also the references therein.

Theorem A.1. *Let* $\mathbf{u}$ *be the solution to* (3) *on a polygonal domain* Ω*. Given* $\mathbf{A}$ *one of the vertices of* Ω*,* $\mathbf{u}$ *admits an asymptotic expansion in polar coordinates at* $\mathbf{A}$ *of the form*

$$\mathbf{u}(r, \theta) = \eta(r) \left[\sum_{i=1}^{M} \sum_{j=0}^{m_i - 1} \mathbf{c}_{i,j} \mathbf{s}_{i,j}(r, \theta) \right] + \mathbf{w}(r, \theta).$$

In the above equation:

- η *denotes a cut-off function, which localises the singular behaviour of the solution;*
- M *is the number of eigenvalues of* $\mathbf{M}$ *with* $\mathbb{R}(\alpha) \in (0, 1)$*, where multiple eigenvalues are counted multiple times accordingly;*
- m_i*, for all* $i = 1, \ldots, M$*, is the length of the Jordan chain corresponding to the eigenfunction* $\mathbf{e}i$*;*
- $\mathbf{c}_{i,j}$ *are suitable coefficients, called* stress intensity factors*, which are explicitly known [27];*
- $\mathbf{s}_{i,j}$ *are the singular functions*

$$\mathbf{s}_{i,j}(r, \omega) = r^{\alpha_i} \sum_{k=0}^{j} \frac{\ln^k(r)}{k!} \mathbf{e}_{i,j-k}(\alpha_i, \theta); \tag{40}$$

- $\mathbf{w}$ *belongs to* H^2 *in a neighbourhood inside* Ω *of* $\mathbf{A}$*.*

Remark 2. As discussed, e.g., in [15, Section 6], if the multiplicity of α is equal to the kernel of the system matrix in (34), then the length of the Jordan chain is one. Consequently, expansion (40) contains no logarithmic factors. This is for instance the case of the L-shaped domain benchmark in Example A.1. In principle, as for the slit domain benchmark in Example A.2, the multiplicity of all the α solving the characteristic equation is 2, which is the dimension of the kernel of the matrix (37). For this reason, we could also compute the second element of the Jordan chain and investigate the behaviour of singular functions containing an extra logarithmic singularity factor.

References

[1] F. Aldakheel, B. Hudobivnik, E. Artioli, L. Beirão da Veiga, and P. Wriggers. Curvilinear virtual elements for contact mechanics. *Comput. Meth. Appl. Mach. Engrg.*, 372:113394, 2020.

[2] E. Artioli, S. Marfia, and E. Sacco. VEM-based tracking algorithm for cohesive/frictional 2D fracture. *Comput. Methods Appl. Mech. Engrg.*, 365:112956, 2020.

[3] E. Artioli and L. Mascotto. Enrichment of the nonconforming virtual element method with singular functions. *Comput. Methods Appl. Mech. Engrg.*, 386:114024, 2021.

[4] B. P. Ayuso de Dios, K. Lipnikov, and G. Manzini. The nonconforming virtual element method. *ESAIM Math. Model. Numer. Anal.*, 50(3):879–904, 2016.

[5] R.E. Barnhill and J.R. Whiteman. Error analysis of Galerkin methods for Dirichlet problems containing boundary singularities. *IMA J. Appl. Math.*, 15(1):121–125, 1975.

[6] L. Beirão da Veiga, F. Brezzi, A. Cangiani, G. Manzini, L.D. Marini, and A. Russo. Basic principles of virtual element methods. *Math. Models Methods Appl. Sci.*, 23(01):199–214, 2013.

[7] L. Beirão da Veiga, A. Chernov, L. Mascotto, and A. Russo. Exponential convergence of the *hp* virtual element method with corner singularity. *Numer. Math.*, 138(3):581–613, 2018.

[8] E. Benvenuti, A. Chiozzi, G. Manzini, and N. Sukumar. Extended virtual element method for the laplace problem with singularities and discontinuities. *Comput. Methods Appl. Mech. Engrg.*, 356:571–597, 2019.

[9] E. Benvenuti, A. Chiozzi, G. Manzini, and N. Sukumar. Extended virtual element method for two-dimensional linear elastic fracture. *Comput. Methods Appl. Mech. Engrg.*, 390:114352, 2022.

[10] Ch. Böhm, L. Munk, B. Hudobivnik, F. Aldakheel, J. Korelc, and P. Wriggers. Virtual elements for computational anisotropic crystal plasticity. *Comput. Meth. Appl. Mach. Engrg.*, 405:115835, 2023.

[11] S. C. Brenner and L. R. Scott. *The mathematical theory of finite element methods*, volume 3. Springer, 2008.

[12] A. Cangiani, E. H. Georgoulis, T. Pryer, and O. J. Sutton. A posteriori error estimates for the virtual element method. *Numer. Math.*, 137(4):857–893, 2017.

[13] M. Costabel and M. Dauge. Computation of corner singularities in linear elasticity. *Lecture notes in pure and applied mathematics*, 1995.

[14] M. Costabel and M. Dauge. Crack singularities for general elliptic systems. *Math. Nachr.*, 235(1):29–49, 2002.

[15] M. Costabel, M. Dauge, and Y. Lafranche. Fast semi-analytic computation of elastic edge singularities. *Comput. Meth. Appl. Mach. Engrg.*, 190(15-17):2111–2134, 2001.

[16] M. Dauge. *Elliptic boundary value problems on corner domains, volume 1341 of Lecture Notes in Mathematics*. Springer-Verlag, Berlin, 1988.

[17] G. Fix. Higher-order Rayleigh-Ritz approximations. *J. Math. Mech.*, 18(7):645–657, 1969.

[18] G. J. Fix, S. Gulati, and G.I. Wakoff. On the use of singular functions with finite element approximations. *J. Comp. Phys.*, 13(2):209–228, 1973.

[19] S. Giani. *hp*-adaptive celatus enriched Discontinuous Galerkin method for second-order elliptic source problems. *SIAM J. Sci. Comp.*, 40(5):B1391–B1418, 2018.

[20] P. Grisvard. *Elliptic problems in nonsmooth domains*. SIAM, 2011.

[21] A. Hussein, F. Aldakheel, B. Hudobivnik, P. Wriggers, P.-A. Guidault, and O. Allix. A computational framework for brittle crack-propagation based on efficient virtual element method. *Finite Elem. Anal. Des.*, 159:15–32, 2019.

[22] A.I. Kalandiia. Remarks on the singularity of elastic solutions near corners. *J. Appl. Math. Mech.*, 33(1):127–131, 1969.

[23] V. A. Kondrat'ev. Boundary value problems for elliptic equations in domains with conical or angular points. *Trudy Moskovskogo Matematicheskogo Obshchestva*, 16:209–292, 1967.

[24] D. Leguillon and E. Sanchez-Palencia. *Computation of singular solutions in elliptic problems and elasticity*. John Wiley & Sons, Inc., 1987.

[25] L. Mascotto. Ill-conditioning in the virtual element method: stabilizations and bases. *Numer. Methods Partial Differential Equations*, 34(4):1258–1281, 2018.

[26] L. Mascotto, I. Perugia, and A. Pichler. Non-conforming harmonic virtual element method: *h*- and *p*-versions. *J. Sci. Comput.*, 77(3):1874–1908, 2018.

[27] V. G. Maz'ya and B. A. Plamenevskii. On the coefficients in the asymptotic of solutions of the elliptic boundary problem in domains with conical points. *Amer. Math. Soc. Trans.*, 123:57–88, 1984.

[28] N. Moës, J. Dolbow, and T. Belytschko. A finite element method for crack growth without remeshing. *Internat. J. Numer. Methods Engrg.*, 46(1):131–150, 1999.

[29] V. M. Nguyen-Thanh, X. Zhuang, H. Nguyen-Xuan, T. Rabczuk, and P. Wriggers. A virtual element method for 2D linear elastic fracture analysis. *Comput. Meth. Appl. Mach. Engrg.*, 340:366–395, 2018.

[30] A. Rössle. Corner singularities and regularity of weak solutions for the two-dimensional Lamé equations on domains with angular corners. *J. Elasticity*, 60(1):57–75, 2000.

[31] T. Strouboulis, I. Babuška, and K. Copps. The design and analysis of the generalized finite element method. *Comput. Methods Appl. Mech. Engrg.*, 181(1-3):43–69, 2000.

[32] L. Yemm. Design and analysis of the extended hybrid high-order method for the Poisson problem. *Adv. Comput. Math.*, 48(4):45, 2022.

[33] B. Zhang, J. Zhao, Y. Yang, and S. Chen. The nonconforming virtual element method for elasticity problems. *J. Comput. Phys.*, 378:394–410, 2019.